Water Organization around Inorganic Nanotubes in Suspension Probed by Polarization-Resolved Second Harmonic Scattering

Gaelle Martin-Gassin, Erwan Paineau, Pascale Launois, Pierre-Marie Gassin

Water Organization Around Inorganic Nanotubes in Suspension Probed by Polarization Resolved Second Harmonic Scattering

Gaelle Martin-Gassin[1], Erwan Paineau[2], Pascale Launois[2], Pierre-Marie Gassin[1]*

1) ICGM, Univ Montpellier, ENSCM, CNRS, Montpellier, France

2) Université Paris-Saclay, CNRS, Laboratoire de Physique des Solides, 91405, Orsay, France

Corresponding Author:

*pierre-marie.gassin@enscm.fr

ABSTRACT

Imogolite nanotube (INT) is a fascinating one-dimensional (1D) material that can be synthesized in liquid phase. Its behavior in solution is crucial for many applications and depends on the organization of water at the liquid-wall interface. We study here this water organization by using the nonlinear optical technique of polarization resolved Second Harmonic Scattering (SHS). A microscopic model is proposed to interpret the origin of the coherent SHS signal recovered in

this 1D colloidal system. This work demonstrates that SHS technique is able to probe the shell of water molecules oriented around the nanotubes. Water organization results from the electric field induced by the nanotube walls and it is strongly dependent of the ionic strength of the suspension.

TOC GRAPHIC
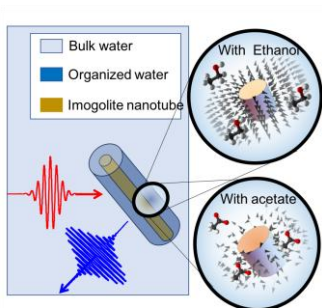
Over the past decade, optical Second Harmonic Scattering (SHS) has demonstrated its ability to probe the surface of colloidal particles in solution[1-8]. SHS is a combination of light scattering technique and Second Harmonic Generation (SHG), a process in which 2 photons at the fundamental frequency are converted in one photon at the harmonic frequency. For charged particles dispersed in a solvent medium, both the solvent molecules adsorbed on the particle surface and those oriented in the Electric Double Layer (EDL) surrounding the particle can generate the second harmonic fields that interfere constructively to give a detectable and coherent SHS signal[9]. This overall signal differs from the one obtained with randomly oriented molecules in a liquid, which results from an incoherent process, namely, hyper-Rayleigh scattering (HRS)[10-14]. In the colloidal field, SHS is able to give microscopic information about the system organization like the number of adsorbed molecules[7], their orientations[1], the length of

the electric double layer[9] or the surface potential[3]. So far, the use of SHS has mostly been restricted to suspensions of spherical nanoparticles[1, 15, 16] and, few work deals with anisotropic suspension[17] like platelets[6] or cylinders[18], this last publication being purely theoretical.

One-dimensional nanoparticles, whose aspect ratio-defined by the ratio of length to diameter-is much higher than one, are the subject of intensive research as interesting building blocks for hierarchical assembly of functional nanostructures[19, 20]. In many cases, their colloidal properties are a crucial aspect for their use. For instance, aqueous two-phase extraction based separation of surfactant dispersed carbon nanotubes, these iconic objects of nanoscience, is in constant progress[21, 22]. It should also be underlined that the colloidal properties of clay nanotubes, a unique class of nanostructured materials, are considered in environmental and industrial applications[23, 24]. Among them, synthetic imogolite nanotubes (INT)[25, 26] constitute a specific case of inorganic hollow nanostructures, truly nanometric in diameter. Understanding water organization around and inside INT represents an essential step for a wide range of applications[26], as catalytic and photocatalytic nanoreactor[27], as liquid crystal[28, 29] or for water depollution[30]. Most experimental and computational works have focused on water confined inside nanotubes[31-35] in the context of the recent development of nanofluidics[36]. Water outside the nanotubes was only studied very near the nanotube, with the modulation of its density profile on a few angstroms and the analysis of nanotube curvature effect on its hydrophilicity[37]. While it is known that imogolite walls are polarized[38, 39], the polarization of water molecules around the nanotubes, has never been addressed, either by numerical computations or experimentally. This may affect the dipole ordering of water molecules. The present study on the structuring of water around imogolite nanotubes by SHS is therefore positioned in a particularly open context, both in

terms of the applicability of the SHS method to 1D colloids and from the perspective of the physical chemistry of imogolite colloids.

The imogolite nanotubes chosen for our investigation are double-walled aluminogermanate nanotube with nominal stoichiometry $GeAl_2O_7H_4$. Their walls are paved with AlO_6 octaedra and GeO_4 tetraedra, as shown in Fig. 1A. Double-walled imogolite nanotubes with different lengths have been synthesized by wet chemical approaches (see Supporting Information for details on the synthesis conditions), to probe the effect of the aspect ratio of these tubular objects on water properties. Two different batches were obtained, referred to as "short INT" and "long INT" batches. In both batches, nanotubes have a monodisperse outer diameter of around 4.4 nm[40, 41]. Transmission electron microscopy (TEM) observations allow for the characterization of length distributions (Figure S1). "Short INT" length distribution follows a log-normal law, the average length being 18 nm and "Long INT" length distribution is found to be bimodal with a contribution of the longest nanotubes around 750 nm. A schematic representation of the experimental setup for SHS measurements is shown in Figure 1B and details about this setup are given in the Supporting Information[6]. The wavelength of the incident beam is fixed at 800 nm. Figures 1C and D present the polarization resolved SHS intensities for the two INT suspension batches with respect to the polarization plots for pure water. The concentration in nanotubes of both suspensions, noted [INT], is fixed at 0.5 g/L, low enough to avoid any orientation effect due to interactions between nanotubes[42].
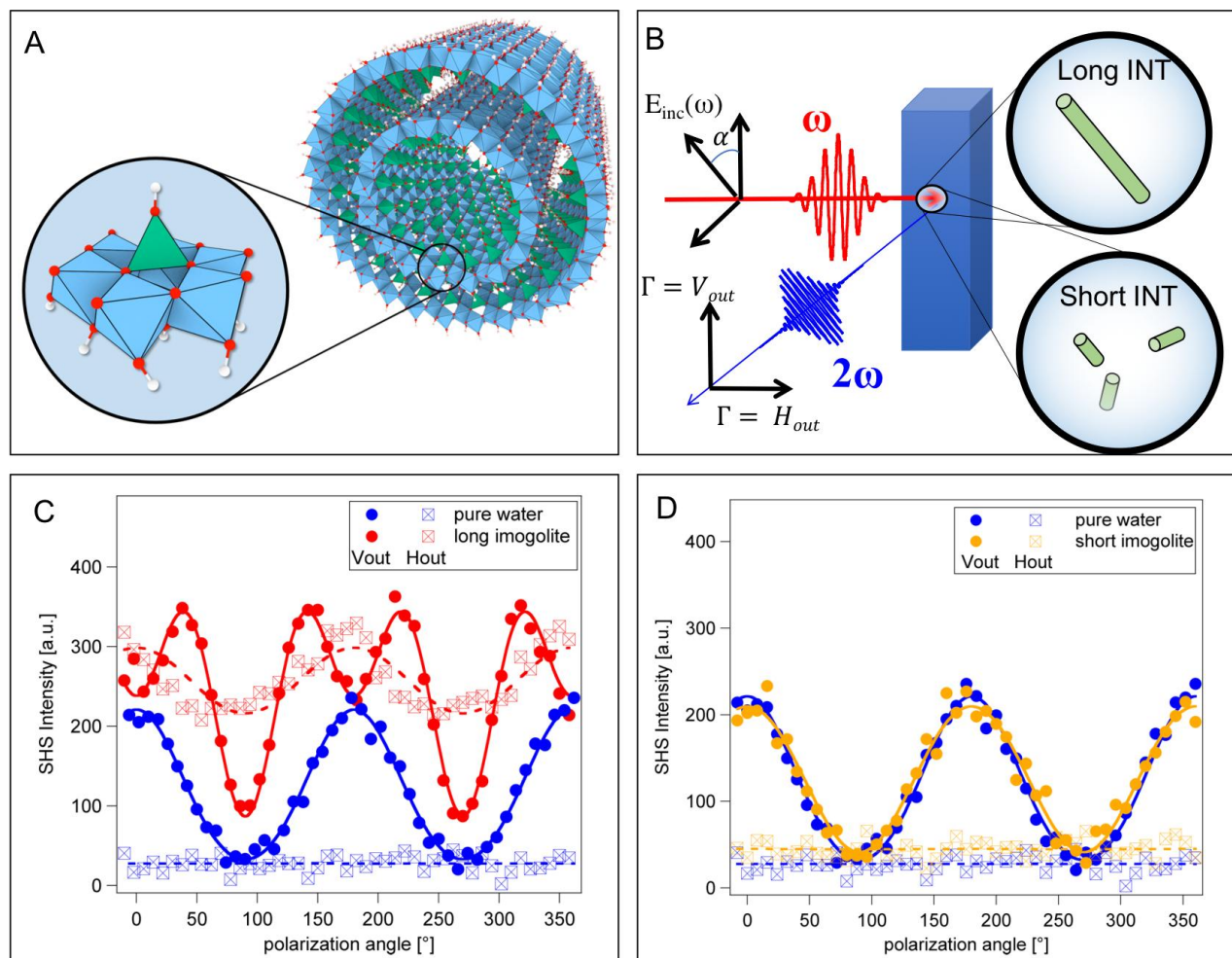
Figure 1. A) Structure of a double-walled aluminogermante INT. AlO_6 octahedra are drawn in blue, GeO_4 tetrahedra in green, oxygen and hydrogen atoms are represented with red and white circles, respectively. B) A schematic representation of the experimental setup, notations used and system studied with long and short INT batches C) SHS polarization plots for pure water in blue and long INT batch suspension ([INT]=0.5g/L) in red. Empty squares correspond to the H_{out} polarization state and full circles to the V_{out} polarization state. The continuous line and dashed lines are fits according to equation (1). D) Same as figure C for the short INT batch suspension ([INT]=0.5g/L) in orange.

The polarization plots differ significantly from those pure water in the case of long INT batch but remains close to pure water for the short INT batch. To discriminate the incoherent and coherent contribution in the whole SHS signal, polarization resolved SHS measurements are analyzed as a function of the input polarization angle α[43], and decomposed in a Fourier series:

$$I_{SHS}(\alpha,\Gamma) = K_{SHS}^{\Gamma}\left(1 + I_{2,SHS}^{\Gamma}\cos(2\alpha) + I_{4,SHS}^{\Gamma}\cos(4\alpha)\right) \quad (1)$$

Here K_{SHS}^{Γ} is a constant, $I_{2,SHS}^{\Gamma}$ and $I_{4,SHS}^{\Gamma}$ are the amplitudes of the second and fourth harmonics in the series, respectively. The index Γ refers to the selection of the second harmonic light either in the vertical (V_{out}) or horizontal (H_{out}) states. The parameter I_2 is related to the local microscopic structure, i.e. the first hyperpolarizability of the water molecule and I_4 to the long-range correlations. In the case of uncorrelated species, SHS is a purely incoherent phenomenon and the amplitude I_4 vanishes[43]. On the contrary, when molecular orientations are correlated, the scattered photons have a well-defined phase relationship and I_4 differs from 0. Experimental coefficients for the two INT batches and bulk water are reported in the three last columns in Table 1. The evolutions of the V_{out} states coefficients as a function of the INT concentration in suspension are drawn in Figure 2 (left). The H_{out} evolutions are not discussed in the following as they are less significative concerning the I_4 coefficient (see Table 1). The SHS signal comes a priori from three different sources: (i) a contribution from bulk water molecules, which is mainly an incoherent contribution, and is referred to as "bulk contribution"; (ii) a coherent contribution coming from water molecules oriented around the INT, named "organized water contribution" and (iii) a contribution of the imogolite itself. We will show in the following that this latter contributes only marginally. Neglecting this contribution, the SHS intensity is written as:

$$I_{SHS}(\alpha,\Gamma) = I_{bulk}(\alpha,\Gamma) + I_{organized}(\alpha,\Gamma) \quad (2)$$

where each term can be developed in a Fourier series:

$$I_{bulk}\ (\alpha, \Gamma) = K_{bulk}^{\Gamma}\left(i_{0,bulk}^{\Gamma} + i_{2,bulk}^{\Gamma}\cos\ (2\alpha) + i_{4,bulk}^{\Gamma}\ \cos(4\alpha)\right) \quad (3)$$

$$I_{organized}\ (\alpha, \Gamma) = K_{organized}^{\Gamma}\left(i_{0,organized}^{\Gamma} + i_{2,organized}^{\Gamma}\cos\ (2\alpha) + i_{4,organized}^{\Gamma}\ \cos\ (4\alpha)\right) (4)$$

The normalized amplitudes in the harmonic development are defined as:

$$I_2^{\Gamma} = \frac{i_2^{\Gamma}}{i_0^{\Gamma}} \quad (5)$$

and $I_4^{\Gamma} = \frac{i_4^{\Gamma}}{i_0^{\Gamma}}$ (6)

The amplitudes $I_{i,\ SHS}^{\Gamma}$ $(i = 2, 4)$ in equation (1) are thus given by:

$$I_{i,\ SHS}^{\Gamma} = \frac{I_{i,bulk}^{\Gamma} + \left(\frac{K_{organized}^{\Gamma}}{K_{bulk}^{\Gamma}}\right)\left(\frac{i_{0,organized}^{\Gamma}}{i_{0,bulk}^{\Gamma}}\right)I_{i,organized}^{\Gamma}}{1 + \left(\frac{K_{organized}^{\Gamma}}{K_{bulk}^{\Gamma}}\right)\left(\frac{i_{0,organized}^{\Gamma}}{i_{0,bulk}^{\Gamma}}\right)} \quad (7)$$

We propose in the following a simple model of the water molecules organization to interpret quantitatively the evolution of $I_{i,\ SHS}^{V}$ amplitudes.
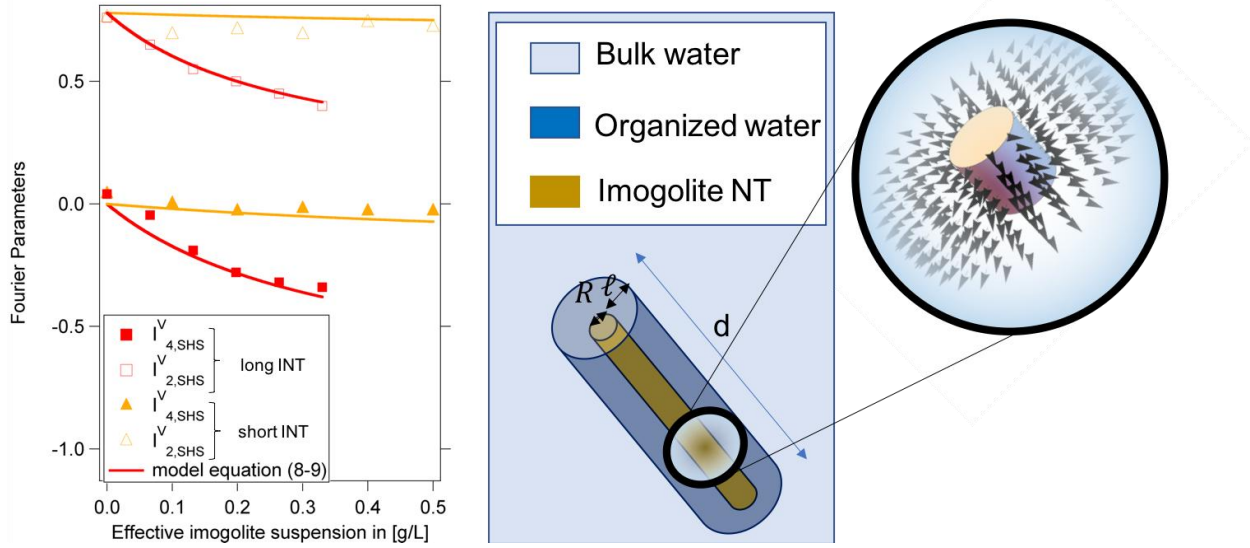
Figure 2. (*Left*) Evolution of the I_2^V and I_4^V amplitudes with the effective suspension concentration as defined in equation S1, for the short and long INT batches: red color for long imogolite batch and orange color for short imogolite batch. The solid line is the model equations (8-9) with the following parameters: R=2.2 nm, $I_{2,\ bulk}^V = 0.78$, $I_{4,\ bulk}^V = 0.00$, d=750 nm, $I_{2,\ organized}^V = 0.10$, $I_{4,\ organized}^V = -0.79$, l=6 nm and $f_2=1.4 \times 10^{-4}$ for long INT batch, and R=2.2 nm, $I_{2,\ bulk}^V = 0.78$, $I_{4,\ bulk}^V = 0.00$, d= 20 nm, $I_{2,\ organized}^V = 0.70$, $I_{4,\ organized}^V = -0.21$, l=6 nm and $f_2=1.4 \times 10^{-3}$ for short INT batch as presented in Table 1. (*Right*) a schematic representation of the model with the *l* and *d* parameters. The arrows in the magnifying glass depict domains of organized water as defined in the computational simulation.

Model of organized water surrounding the INT. The nanotubes are modeled with a monodisperse length d=20 nm or 750 nm for short and long INT batches respectively. The organized water contribution is modeled by a cylindrical shell of oriented water molecules surrounding the INT, as depicted in Figure 2. The harmonics amplitudes $I_{i,\ SHS}^\Gamma$ are expressed as a function of the shell extension ℓ in the radial direction. Under these assumptions, the equation (7) becomes:

$$I_{i,SHS}^{\Gamma} = \frac{I_{i,bulk}^{\Gamma} + f_1([INT],d,\ell) \times f_2(d,l) \times I_{i,organized}^{\Gamma}}{1 + f_1([INT],d,\ell) \times f_2(d,l)} \quad (8)$$

where $f_1([INT],d,\ell) = \frac{[INT]}{\mu_{INT}} \times \rho_{water} \times \pi^2 \times d \times (\ell^2 + 2\ell R)^2$ (9)

Here R is the nanotube radius taken to 2.2 nm, μ_{INT} is the linear mass of the INT, ρ_{water} is the water density, [INT] is the imogolite suspension concentration in g/L. The $f_2(d,l)$ factor is the ratio between $i_{0,organized}$ and $i_{0,bulk}$ and additional details are given in SI to calculate its value. As the bulk contribution is considered as mainly incoherent, the $I_{i,bulk}^{\Gamma}$ coefficients depends only of the water hyperpolarizability, while the $I_{i,organized}^{\Gamma}$ coefficients are evaluated with a computational program[44, 45] based on a microscopic model of water domains oriented radially around the INT (see details in SI). The inputs of this program are the hyperpolarizability of the water molecule and the position and orientation of each water domain. A significant number of around 20000 water domains are placed in the shell as depicted by the arrows in Figure 2. The characteristic size of the water domains must be small enough compared to the incident laser wavelength in order to account properly for the field retardation effect.[43] As shown in Table S1, the numerical outputs of the computational simulation do not depend of the domain volume provided it is smaller than 100 nm^3, which is thus the maximum volume used. The hyperpolarizability of water $\beta^{(2)}$ used in the computational program is[46]: $\beta_{zzz} = -14.50$ $\beta_{zxx} = -10.25$ $\beta_{xxz} = -10.18$ $\beta_{zyy} = -5.83$ $\beta_{yyz} = -7.59$. All these values are given in atomic units where 1 a.u. = 3.206 *10^{-53} C^{3}m^{3}J^{-2}. The coefficients I_i^{Γ} computed by the model are presented in Table 1 for both the long and short INT batches.

Table 1. The I_i^Γ values computed for suspensions at 0.5g/L, with l=6 nm and d=750 nm for long INT batch and d=20 nm for short INT batch, versus the experimental values. The $I_{i,bulk}^\Gamma$ and $I_{i,organized}^\Gamma$ are computed with the PySHS program, the $I_{i,SHS}^\Gamma$ values are obtained using equations (8-9). For experimental results, the errors bars in the I_i^Γ parameters are evaluated to +- 0.02 by a repeatability study.

	Computational model long INT			Computational model short INT			Experiments		
	I_{bulk}	$I_{organized}$	I_{SHS}	I_{bulk}	$I_{organized}$	I_{SHS}	Pure water	long INT	short INT
I_2^V	0.78	0.10	0.34	0.78	0.70	0.75	0.77	0.30	0.74
I_4^V	0.00	-0.79	-0.41	0.00	-0.21	-0.05	0.04	-0.36	-0.02
I_2^H	0.00	0.60	0.25	0.00	0.03	0.00	0.00	0.19	0.00
I_4^H	0.00	0.04	0.03	0.00	0.00	0.00	0.00	0.05	0.00

Discussion about modelling and experiments. The experimental polar plot of pure water gives numerical values of $I_{i,SHS}^\Gamma$ close to those predict with the model of incoherent water. The very weak positive value of I_4^V found for experiments performed on bulk water may be due by long range orientational correlations in liquid water[43]. The evolutions of $I_{i,SHS}^\Gamma$ with the concentration in mass of the nanotubes (Figure 2) and the nanotube size (table 1) are well reproduced with the model for a shell extension ℓ around 6 nm. This size can be compared to the Debye length[47]:

$$\ell_D = \frac{\kappa^{-1}}{\sqrt{C_{el}}} = \frac{\kappa^{-1}}{\sqrt{C_{res} + C_{add}}} \quad (10)$$

where C_{el} is the electrolyte concentration, with $\kappa^{-1} = 304.9$ for C_{el} in µmol/L and ℓ_D in nm; the electrolyte concentration is the sum of a concentration of residual ions coming from the synthesis ($C_{res} \simeq 100$ µmol/L, see SI) and of the concentration of electrolyte possibly added further (C_{add}). The simple model of anisotropic objects assuming at the first order a monodisperse distribution for the d parameter describing the size of the INT is able to well reproduced all the experimental data, without any fit and for a shell extension parameter l set around 6 nm. The origin of a high negative value in the $I_4{}^V$ parameters is clearly attributed to the orientation of water on this characteristic length which is about a fifth of the Debye length in this condition.

Effect of the ionic strength on the surrounding water shell. Figure 3A presents the evolution of the V_{out} polarization plot under the NaCl salt addition for suspensions of long INT. The evolution of $I_{4,SHS}^V$ parameter, determined according to equation (1), is presented in Figure 3B as a function of the addition of various inorganic, organic, weak or strong electrolytes but also of non-electrolyte solutions. For all the inorganics electrolytes tested here, i.e. NaCl, $CsNO_3$, HCl, NaSCN, the evolution is nearly the same with a large change in the $I_4{}^V{}_{SHS}$ parameter under the 10-100 µM ion addition range. At ionic strength higher than 0.5 mM (see green data in Figure 3A) the polarization plots are similar to the signal obtained for pure liquid water shown in Figure 1A. This result validates the above assumption that imogolite does not exhibit any intrinsic nonlinear response and that the difference in the polarization plots comes from the oriented and organized water domain surrounding the INT. The solid lines in Figure 3B represents the $I_4{}^V{}_{SHS}$ parameter computed with the model equations (8-9). It reveals that the size of the oriented water domains decreases and falls to zero with the addition of ionic species in line with the decrease of

the Debye length. Moreover, our experimental results are independent of the chemical nature of the ion pairs studied demonstrating the effectiveness of the SHS signal in probing the organized water in the first layer. To go further, the effect of adding non-electrolyte molecule like ethanol or weak organic electrolyte compounds (acetic CH_3COOH and formic CH_2O_2 acids) has been investigated. In this last case, the quantity of electrolyte added in the suspension is estimated by solving numerically the quadratic weak acid equation, which is written:

$$K_a = \frac{[X]^2}{C_{acid}-[X]} \quad (11)$$

where X= CH_3COO^- or $CHOO^-$, [X] is the molar concentration in X species, K_a is the acid constant equal to 3.75 for formic acid and 4.75 for acetic acid and C_{acid} is the molar concentration addition of the acid species. The results are the same as for the inorganic ions, which confirms the conclusion done on these species. On the contrary, in the case of ethanol, the $I^V_{4,SHS}$ parameter remains constant, showing that such non-ionic molecules do not play any role in the water organization around the INT.
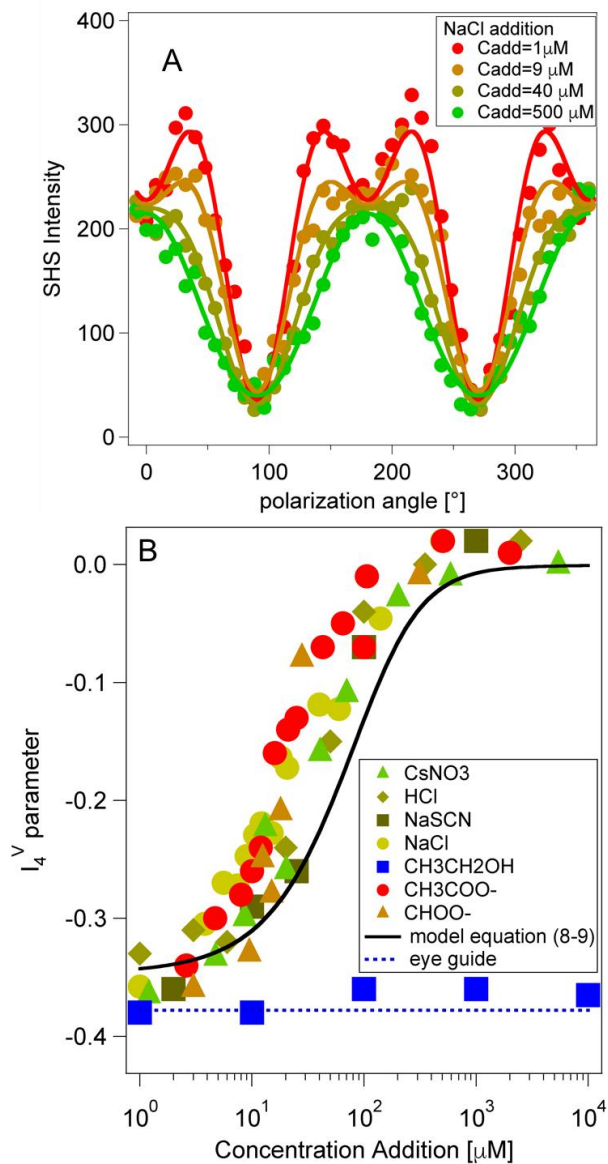
Figure 3. A) V_{out} polarization plot for NaCl salt addition in the long imogolite suspension at 0.5 g/L. B) The $I_{4,SHS}^V$ evolution after different compounds addition in the long INT suspension at 0.5 g/L. The black solid line is the model equations (8-9) with the following parameters d=750 nm, R=2.2 nm, [INT]=0.5 g/L, $I_{4,bulk}^V$= 0.00, $I_{4,organized}^V$= -0.79, $\ell = \frac{\ell_D}{5}$. For formic and acetic acid addition, the quantity of CHCOO⁻ or CH_3COO^- ions is estimated according equation (11).

In summary, this letter highlights for the first time the relevance and potential of the SHS technique in probing the water organization around 1D imogolite nanotubes in suspension. The SHS measurements are analyzed in terms of coherent and incoherent SHS contributions. The model developed here is able to compute both contributions from microscopic organization, allowing a direct comparison from the experimental data obtained on suspensions of INTs with different aspect ratio. The modeling demonstrates that the SHS coherent contribution observed for highly anisometric nanotubes arises from the radially oriented water molecules surrounding the nanotube. At low ionic strength, those molecules are aligned with the electric field coming from the charged INT wall on a distance in the range of 5-6 nm. The I_4^V parameter exhibits large variation for ionic strength in the 10-100 μM range for long INTs. This parameter is independent of the chemical nature of the monovalent ion pairs studied here but it remains constant when non-ionic molecules like ethanol are added in the suspension. The model and the related numerical code developed here are quite general and open new perspectives to probe the electric double layer extension in any 1D colloidal system.

ASSOCIATED CONTENT

Supporting Information. Additional information about Imogolite synthesis and characterization, evaluation of the long imogolite mass concentration in urea batch, SHS experimental setup, derivation of the model of bulk and organized water, the computational model used to calculate the $I_{i,organized}^{\Gamma}$ and $i_{0,organized}^{\Gamma}$ parameters, and additional polarization resolved plots predicted by the model for different length l. The following files are available free of charge.

REFERENCES

1.   Roke, S.; Gonella, G., Nonlinear Light Scattering and Spectroscopy of Particles and Droplets in Liquids. *Annual Review of Physical Chemistry* **2012,** *63* (1), 353-378.
2.   Yan, E. C. Y.; Eisenthal, K. B., Probing the Interface of Microscopic Clay Particles in Aqueous Solution by Second Harmonic Generation. *The Journal of Physical Chemistry B* **1999,** *103* (29), 6056-6060.
3.   Yan, E. C. Y.; Liu, Y.; Eisenthal, K. B., New Method for Determination of Surface Potential of Microscopic Particles by Second Harmonic Generation. *The Journal of Physical Chemistry B* **1998,** *102* (33), 6331-6336.
4.   Lütgebaucks, C.; Gonella, G.; Roke, S., Optical label-free and model-free probe of the surface potential of nanoscale and microscopic objects in aqueous solution. *Physical Review B* **2016,** *94* (19), 195410.
5.   Marchioro, A.; Bischoff, M.; Lütgebaucks, C.; Biriukov, D.; Předota, M.; Roke, S., Surface Characterization of Colloidal Silica Nanoparticles by Second Harmonic Scattering: Quantifying the Surface Potential and Interfacial Water Order. *The Journal of Physical Chemistry C* **2019,** *123* (33), 20393-20404.
6.   Gassin, P.-M.; Prelot, B.; Gregoire, B.; Martin-Gassin, G., Second-Harmonic Scattering Can Probe Hydration and Specific Ion Effects in Clay Particles. *The Journal of Physical Chemistry C* **2020,** *124* (7), 4109-4113.
7.   Das, A.; Chakrabarti, A.; Das, P. K., Probing protein adsorption on a nanoparticle surface using second harmonic light scattering. *Physical Chemistry Chemical Physics* **2016,** *18* (35), 24325-24331.
8.   Bernhard, C.; van Zadel, M.-J.; Bunn, A.; Bonn, M.; Gonella, G., In Situ Label-Free Study of Protein Adsorption on Nanoparticles. *The Journal of Physical Chemistry B* **2021,** *125* (31), 9019-9026.
9.   Gonella, G.; Lütgebaucks, C.; de Beer, A. G. F.; Roke, S., Second Harmonic and Sum-Frequency Generation from Aqueous Interfaces Is Modulated by Interference. *The Journal of Physical Chemistry C* **2016,** *120* (17), 9165-9173.
10.   Tocci, G.; Liang, C.; Wilkins, D. M.; Roke, S.; Ceriotti, M., Second-Harmonic Scattering as a Probe of Structural Correlations in Liquids. *The Journal of Physical Chemistry Letters* **2016,** *7* (21), 4311-4316.

11.   Duboisset, J.; Rondepierre, F.; Brevet, P.-F., Long-Range Orientational Organization of Dipolar and Steric Liquids. *The Journal of Physical Chemistry Letters* **2020,** *11* (22), 9869-9875.

12.   Borgis, D.; Belloni, L.; Levesque, M., What Does Second-Harmonic Scattering Measure in Diluted Electrolytes? *The Journal of Physical Chemistry Letters* **2018,** *9* (13), 3698-3702.

13.   Shelton, D. P., Long-range orientation correlation in water. *The Journal of Chemical Physics* **2014,** *141* (22), 224506.

14.   Shelton, D. P., Long-range orientation correlation in dipolar liquids probed by hyper-Rayleigh scattering. *The Journal of Chemical Physics* **2015,** *143* (13), 134503.

15.   Eisenthal, K. B., Second Harmonic Spectroscopy of Aqueous Nano- and Microparticle Interfaces. *Chemical Reviews* **2006,** *106* (4), 1462-1477.

16.   Gonella, G.; Dai, H.-L., Second Harmonic Light Scattering from the Surface of Colloidal Objects: Theory and Applications. *Langmuir* **2014,** *30* (10), 2588-2599.

17.   de Beer, A. G. F.; Roke, S.; Dadap, J. I., Theory of optical second-harmonic and sum-frequency scattering from arbitrarily shaped particles. *J. Opt. Soc. Am. B* **2011,** *28* (6), 1374-1384.

18.   Dadap, J. I., Optical second-harmonic scattering from cylindrical particles. *Physical Review B* **2008,** *78* (20), 205322.

19.   Serra, M.; Arenal, R.; Tenne, R., An overview of the recent advances in inorganic nanotubes. *Nanoscale* **2019,** *11* (17), 8073-8090.

20.   Xia, Y.; Yang, P.; Sun, Y.; Wu, Y.; Mayers, B.; Gates, B.; Yin, Y.; Kim, F.; Yan, H., One-Dimensional Nanostructures: Synthesis, Characterization, and Applications. *Advanced Materials* **2003,** *15* (5), 353-389.

21.   Fagan, J. A., Aqueous two-polymer phase extraction of single-wall carbon nanotubes using surfactants. *Nanoscale Advances* **2019,** *1* (9), 3307-3324.

22.   Defillet, J.; Avramenko, M.; Martinati, M.; López Carrillo, M. Á.; Van der Elst, D.; Wenseleers, W.; Cambré, S., The role of the bile salt surfactant sodium deoxycholate in aqueous two-phase separation of single-wall carbon nanotubes revealed by systematic parameter variations. *Carbon* **2022,** *195*, 349-363.

23.   Yuan, P.; Tan, D.; Annabi-Bergaya, F., Properties and applications of halloysite nanotubes: recent research advances and future prospects. *Applied Clay Science* **2015,** *112-113*, 75-93.

24.   Lazzara, G.; Cavallaro, G.; Panchal, A.; Fakhrullin, R.; Stavitskaya, A.; Vinokurov, V.; Lvov, Y., An assembly of organic-inorganic composites using halloysite clay nanotubes. *Current Opinion in Colloid & Interface Science* **2018,** *35*, 42-50.

25.   Guimarães, L.; Enyashin, A. N.; Frenzel, J.; Heine, T.; Duarte, H. A.; Seifert, G., Imogolite Nanotubes: Stability, Electronic, and Mechanical Properties. *ACS Nano* **2007,** *1* (4), 362-368.

26.   Paineau, E., Imogolite Nanotubes: A Flexible Nanoplatform with Multipurpose Applications. *Applied Sciences* **2018,** *8* (10).

27.   Elliott, J. D.; Poli, E.; Scivetti, I.; Ratcliff, L. E.; Andrinopoulos, L.; Dziedzic, J.; Hine, N. D. M.; Mostofi, A. A.; Skylaris, C.-K.; Haynes, P. D.; Teobaldi, G., Chemically Selective Alternatives to Photoferroelectrics for Polarization-Enhanced Photocatalysis: The Untapped Potential of Hybrid Inorganic Nanotubes. *Advanced Science* **2017,** *4* (2), 1600153.

28.   Paineau, E.; Krapf, M.-E. M.; Amara, M.-S.; Matskova, N. V.; Dozov, I.; Rouzière, S.; Thill, A.; Launois, P.; Davidson, P., A liquid-crystalline hexagonal columnar phase in highly-dilute suspensions of imogolite nanotubes. *Nat Commun* **2016,** *7* (1), 10271.

29.   Su, C.-Y.; Lyu, Q.; Kang, D.-Y.; Yang, Z.-H.; Lam, C. H.; Chen, Y.-H.; Lo, S.-C.; Hua, C.-C.; Lin, L.-C., Hexagonal Superalignment of Nano-Objects with Tunable Separation in a Dilute and Spacer-Free Solution. *Physical Review Letters* **2019,** *123* (23), 238002.

30.   Amara, M. S.; Paineau, E.; Rouzière, S.; Guiose, B.; Krapf, M.-E. M.; Taché, O.; Launois, P.; Thill, A., Hybrid, Tunable-Diameter, Metal Oxide Nanotubes for Trapping of Organic Molecules. *Chemistry of Materials* **2015,** *27* (5), 1488-1494.

31.   Creton, B.; Bougeard, D.; Smirnov, K. S.; Guilment, J.; Poncelet, O., Molecular dynamics study of hydrated imogolite 2. Structure and dynamics of confined water. *Physical Chemistry Chemical Physics* **2008,** *10* (32), 4879-4888.

32.   Konduri, S.; Tong, H. M.; Chempath, S.; Nair, S., Water in Single-Walled Aluminosilicate Nanotubes: Diffusion and Adsorption Properties. *The Journal of Physical Chemistry C* **2008,** *112* (39), 15367-15374.

33.   Belorizky, E.; Fries, P. H.; Guillermo, A.; Poncelet, O., Almost ideal 1D water diffusion in imogolite nanotubes evidenced by NMR relaxometry. *Chemphyschem : a European journal of chemical physics and physical chemistry* **2010,** *11 9*, 2021-6.

34.   González, R. I.; Rojas-Nunez, J.; Valencia, F. J.; Munoz, F.; Baltazar, S. E.; Allende, S.; Rogan, J.; Valdivia, J. A.; Kiwi, M.; Ramírez, R.; Greathouse, J. A., Imogolite in water: Simulating the effects of nanotube curvature on structure and dynamics. *Applied Clay Science* **2020,** *191*, 105582.

35.   Scalfi, L.; Fraux, G.; Boutin, A.; Coudert, F.-X., Structure and Dynamics of Water Confined in Imogolite Nanotubes. *Langmuir* **2018,** *34* (23), 6748-6756.

36.   Bocquet, L., Nanofluidics coming of age. *Nature Materials* **2020,** *19* (3), 254-256.

37.   Fernandez-Martinez, A.; Tao, J.; Wallace, A. F.; Bourg, I. C.; Johnson, M. R.; De Yoreo, J. J.; Sposito, G.; Cuello, G. J.; Charlet, L., Curvature-induced hydrophobicity at imogolite–water interfaces. *Environmental Science: Nano* **2020,** *7* (9), 2759-2772.

38.   Teobaldi, G.; Beglitis, N. S.; Fisher, A. J.; Zerbetto, F.; Hofer, W. A., Hydroxyl vacancies in single-walled aluminosilicate and aluminogermanate nanotubes. *Journal of Physics: Condensed Matter* **2009,** *21* (19), 195301.

39.   Monet, G.; Paineau, E.; Chai, Z.; Amara, M. S.; Orecchini, A.; Jimenéz-Ruiz, M.; Ruiz-Caridad, A.; Fine, L.; Rouzière, S.; Liu, L.-M.; Teobaldi, G.; Rols, S.; Launois, P., Solid wetting-layers in inorganic nano-reactors: the water in imogolite nanotube case. *Nanoscale Advances* **2020,** *2* (5), 1869-1877.

40.   Amara, M.-S.; Paineau, E.; Bacia-Verloop, M.; Krapf, M.-E. M.; Davidson, P.; Belloni, L.; Levard, C.; Rose, J.; Launois, P.; Thill, A., Single-step formation of micron long (OH)3Al2O3Ge(OH) imogolite-like nanotubes. *Chemical Communications* **2013,** *49* (96), 11284-11286.

41.   Paineau, E.; Monet, G.; Peyre, V.; Goldmann, C.; Rouzière, S.; Launois, P., Colloidal Stability of Imogolite Nanotube Dispersions: A Phase Diagram Study. *Langmuir* **2019,** *35* (38), 12451-12459.

42.   Paineau, E.; Rouzière, S.; Monet, G.; Diogo, C. C.; Morfin, I.; Launois, P., Role of initial precursors on the liquid-crystalline phase behavior of synthetic aluminogermanate imogolite nanotubes. *J. Colloid Interface Sci.* **2020,** *580*, 275-285.

43.   Duboisset, J.; Brevet, P.-F., Salt-induced Long-to-Short Range Orientational Transition in Water. *Physical Review Letters* **2018,** *120* (26), 263001.

44.   Boudjema, L.; Aarrass, H.; Assaf, M.; Morille, M.; Martin-Gassin, G.; Gassin, P.-M., PySHS: Python Open Source Software for Second Harmonic Scattering. *Journal of Chemical Information and Modeling* **2020,** *60* (12), 5912-5917.

45.   Boudjema, L.; Aarrass, H.; Assaf, M.; Morille, M.; Martin-Gassin, G.; Gassin, P.-M., Correction to "PySHS: Python Open Source Software for Second Harmonic Scattering". *Journal of Chemical Information and Modeling* **2021,** *61* (11), 5719-5719.

46.   Luo, Y.; Ågren, H.; Vahtras, O.; Jo/rgensen, P.; Spirko, V.; Hettema, H., Frequency-dependent polarizabilities and first hyperpolarizabilities of H2O. *The Journal of Chemical Physics* **1993,** *98* (9), 7159-7164.

47.   Israelachvili, J. N., 14 - Electrostatic Forces between Surfaces in Liquids. In *Intermolecular and Surface Forces (Third Edition)*, Israelachvili, J. N., Ed. Academic Press: Boston, 2011; pp 291-340.